Compact Accumulation Radar for Thwaites MELT

John PADEN,[1] Fernando RODRIGUEZ-MORALES,[1] Carl ROBINSON,[2] Alejandra ESCALERA,[1] Richard HALE,[1] Tom JORDAN,[2] Krishnateja KARIDI,[1] Cameron LEWIS,[1] Keith NICHOLS,[2] David PORTER,[3] BRadley SCHROEDER,[1] Jianxuan SHANG,[1] Hara TALASILA[1]

[1]*Center for Remote Sensing of Ice Sheets, University of Kansas, Lawrence, KS, USA*

[2]*British Antarctic Survey, High Cross, Madingley Road, Cambridge, UK*

[3]*Lamont Doherty Earth Observatory, 61 Rte 9W, Palisades, NY, USA*

Correspondence: John Paden <paden@cresis.ku.edu>

ABSTRACT. We developed and deployed a compact two channel radar sounder for phase sensitive repeat pass displacement measurements of basal melt and snow layers for accumulation rate measurements. The radar operates from 600 MHz to 900 MHz with a 400W transmitter. This frequency range has sufficient penetration for thin ice and enables the use of a small antenna array that can be installed in the limited space underneath the floor of a Twin Otter aircraft. We detail the system electronics and antenna including the various calibration mechanisms built in to monitor phase stability and system health. The system includes two channels to simultaneously capture a low gain and high gain version of the signal so that the strong surface and shallow layer scattering as well as weak ice bottom and deep layer returns can be captured. The radar system was integrated onto a British Antarctic Survey (BAS) Twin Otter as part of the NSF-NERC Thwaites MELT project and deployed in 2018-2019 with plans to repeat measurements one year later during the 2019-2020 austral summer. We present results from the 2019 survey, evaluate the radar's noise and radiometric performance, and demonstrate the antennas-in-the-loop system impulse response.

INTRODUCTION

Purpose of measurements (proposal: melt rates and layers accumulation, investigate firn compaction and vertical strain, bathymetry, grounding line,)

HARDWARE DESCRIPTION

The radar system is composed of four main sections: power conditioning, high-speed mixed-signal section, RF section, and antennas. A simplified system block diagram is shown in Fig. 1. The power section conditions the signal from the aircraft's DC generator and produces all the voltages required for operation. It consists of an external uninterruptible power supply (UPS), power filter modules, and a bank of switching DC-DC converters and regulators. The high-speed mixed signal section is based on modules from the Arena 300 series from Remote Sensing Solutions (RSS) [1]. Besides custom clock generation/distribution circuitry synchronous to a master 10-MHz source, this section includes an arbitrary waveform generator (AWG), a central timing unit (CTU) for control and synchronization, and two high-speed analog-to-digital converter (ADC) channels. The AWG runs at 2 GSa/s to directly synthesize wideband pulsed chirp signals in the 600 MHz to 900 MHz range. The ADCs operate at 1 GSa/s with an internal clock divider. We use x2 onboard decimation to achieve an effective sampling rate of 500 MSa/s. The radar records 16-bit I/Q baseband samples with a coordinated universal time (UTC) stamp from an onboard global positioning system (GPS) receiver. We use 48 hardware presums to reduce the data rate and enable multi-hour acquisitions (data rate 25 MB/s). The radar is controlled from a laptop computer running a custom graphical user interface. The RF section consists of a high-power transmit/receive (T/R) module and a dual-channel analog receiver. The T/R module is a custom design with low insertion loss that allows sharing the same antenna for transmission and reception, handling high peak RF power levels with a duty cycle of up to 10

ANTENNA INTEGRATION

Structural Design Requirements

Most of the structural design requirements for this system were derived from instrument performance. A major design driver was minimizing the deflection of the mounting plate around the LIDAR. The maximum deflection of the LIDAR could not increase by more than 0.1 mm, compared to the previous LIDAR mount. The previous LIDAR mounting plate was analyzed for comparison to verify the maximum deflection of the

Table 1. Summary of system parameters

Parameters	Value	Units
Operating frequency range	600 to 900	MHz
Range resolution (air, no window)	0.5	m
Peak transmit power	400	Watt
Pulse duration (programmable)	2	μs
Pulse repetition frequency (typ.)	25	kHz
Sampling rates	2.0 (AWG) / 1.0 (ADCs)	GS/s
Transmit channels	1	
Receive channels	2 (low-gain/high-gain)	
Antenna type	Vivaldi array	
Antenna array gain	6	dBi
Radar system weight	25	kg
Power consumption	300	Watt

LIDAR would not exceed this limit under any loading condition.

The design was also heavily influenced by the geometry of the Twin Otter camera bay. The perimeter geometry of the mounting plate was fixed based on the dimensions of the Twin Otter camera bay and the corresponding hardpoints. For mounting, the maximum load on the hardpoints could not exceed 534 N (120 lbs), as outlined in the British Antarctic Survey documentation(BAS, 1994). Also, since the mounting plate is integrated directly into the structure of the aircraft, ultimate load failure analysis was performed with a factor of safety (FS) of 1.5.

Another major contributing factor to the design was the schedule of the project, requiring a design which could be easily manufactured. The design included stock sizes of metallic components made of 2024-T3, 2024-T351, and 6061-T6 which were readily available or could be acquired rapidly. Composite components were used in regions parallel to the antenna array and below the mounting plate to mitigate any reduction in antenna performance. The composite components were made of S2-glass fiber and the geometry was based on existing composite tooling for rapid manufacturing.

Table 2. Inertial load cases for analyzing the BAS Twin Otter camera bay

Load Case	Inertial Loads	Source(BAS, 1994)(FAA, 2018)
1	10.35G Forward	BAS
2	1.725G Rearward	BAS
3	5.175G Upward	BAS
4	6G Downward	BAS
5	3G Sideward	BAS
-	1G Downward	-

Loads

Five different inertial load cases were considered during the analysis of the combined LIDAR and accumulation radar antenna array system. The load cases were derived from both the BAS documentation(BAS, 1994) and the Federal Aviation Administration's (FAA) crash loads documentation(FAA, 2018). The most extreme load case in each direction was selected for a conservative analysis approach. The final load cases and the corresponding sources are summarized in Table 2. The 1G downward load case was used to determine the weight of the final design of the mounting plate.

Analysis and Verification

The geometry of the camera bay plate, LIDAR, accumulation radar antenna array, and antenna housing was created in Unigraphics NX 12(uni, ????). MSC Patran/NASTRAN software(pat, ????) was used to create the finite element models for both the previous LIDAR mount and the final system.

Finite Element Analysis

Every structural component was evaluated for all load cases using finite element software MSC Patran/NASTRAN. Two-dimensional shell elements were used to model all components except for metal extrusions. Extrusions were modeled as one-dimensional beams. The inertial loads were applied to the finite element model as global loads and every component was analyzed for all possible failure modes (tension, compression, buckling and shear). A factor of safety of 1.5 was added to the Margin of Safety (MS) calculations.

A maximum stress criterion was used to evaluate the fiber reinforced structures against failure. Open-

Table 3. Increase in Maximum Deflection of LIDAR mount Load Case

Load Case	Change in Maximum Deflection (mm)
10.35G Forward	0.005
1.725G Rearward	0.001
5.175G Upward	0.032
6G Downward	0.036
3G Sideward	0.000

hole allowables were used for the analysis of composite structures. A-basis allowables outlined in Military Handbook 5H(mil, 1998) were used for all metal parts. For a conservative approach, the lower value between the L and LT basis was used for MS calculations. Standard MS calculations were performed using equation 1. All structures were sized to a positive margin of safety.

$$MS = \frac{\sigma_{allowable}}{1.5\sigma_{actual}} - 1 \tag{1}$$

A static analysis was performed for each load case to analyze the maximum deflection of the system. The deflection of the mounting plate had to remain within 0.1 mm of the maximum deflection of the previous LIDAR mounting plate. Table 3 includes the increase in deflection of the mounting plate for each load case. The weight of the final design is 30.1 kg.

High margins of safety were calculated for all possible fastener locations in both the metallic and composite components. Because of the high margins of safety a minimum number of fasteners were required, and the main design concern was edge distance and fastener-to-fastener spacing due to volume constraints of the system. All fastener patterns were designed to adhere to appropriate minimum edge and fastener-to-fastener spacing rules. For metallic and composite materials, fastener-to-fastener spacing was required to be 4D and 5D, respectively. Minimum edge spacing for composite materials was required to be 3D, while minimum edge spacing for metal materials was required to be 2D.

In addition to the static analysis, modal analysis was performed. For the modal analysis, all modes were required to be outside the Blade Passage Frequency (BPF) of the Twin Otter by 5 Hz. The blade passage frequencies used for this analysis were 81.4 Hz, and 99 Hz, each corresponding to a different mode of flight: Normal Operations, and Climb, respectively. When performing the analysis, bounds were set for the modal analysis to only analyze frequencies in a range around the blade passage frequencies.

Table 4. Predicted and measured modal response

Blade passage frequency (Hz)	Predicted frequency (Hz)	Frequency measured (Hz)
81.4	87	76.6, 89.7
99	92	89.7, 107

Modal Testing

The finite element model of the system was used to predict the natural frequencies which were close to the blade passage frequencies and their corresponding mode shapes. The first modes found in the finite element model were bending modes for the lid of the antenna housing. The finite element analysis did not show any structural resonance frequencies in the ranges of 81.4 ± 5 Hz, or 99 ± 5 Hz.

The final system was subjected to modal testing. A mechanical shaker was used to generate random excitation. The input force was measured by a force transducer and the response was measured by several accelerometers. For modal testing, the shaker and the accelerometers were positioned based on the responses generated in the finite element analysis. Table 4 shows the results of the modal testing.

After performing modal testing only one resonance was observed within 81.4 ± 5 Hz, at 76.6 Hz. The tests verified there were no structural resonances in the 99 ± 5 Hz range. During modal testing the LIDAR was not available and an aluminum beam was added in place of the LIDAR. This was taken into account in the finite element analysis. The modal testing produced similar results to what was predicted and it also produced extra modes. The probable cause of these extra frequencies is a difference in the boundary conditions between the finite element model and the actual test setup. Overall, the predicted and measured results provide sufficient validation of the structural analysis.

DISCUSSION AND RESULTS

CONCLUSION

In the IGS design, shortened versions of the title and authors are used in the running head. The shortened version is specified in square braces immediately after the `\title` and `\author` commands (see below).

```
\title[Short Title]{The Full Title of Your Paper}
\author[Short Authors]{Author 1, Author 2 and Author 3}
```

Table 5. One-column table captions will extend beyond the rules in two-column format. Do not try to adjust! Table captions do not have full points at the end

Period[a]	Surface elevation change	Emergence velocity
1975–85	−0.50	0.43
1986–2002	−1.03	0.32
Difference	−0.53	−0.11

[a]Please do not use more than one '&' between columns, and note that if a table includes table footnotes, it must be inside a `minipage` environment.

Lists

The IGS class file provides for numbered (`enumerate`) and unnumbered (`itemize`) lists. Nested lists are not encouraged. The default numbering system is 1., 2., 3., etc.; please do not change this unless there is a good reason. The IGS design removes bullet points from unnumbered lists.

User-defined macros

If possible, please do not define any new macros.

Tables

Tables may be typeset in either one- or two-column format. To typeset two-column format, add asterisks (`\begin{table*}...\end{table*}`) as shown in Table 6. We may change the format in-house if necessary. Please avoid the use of colour or shading. Note that if you choose to refer to tables using labels, `\caption` must precede `\label`, as in standard LaTeX. Vertical rules are not house-style and will be removed. Note the use of the minipage environment in Table 5 which enables table footnotes to be output. If the table is two-column, use `{178mm}` instead of `{86mm}` on line 6. The source code for Tables 5 and 6 is shown immediately below the tables.

Figures

Figures may be typeset in either one- or two-column format. One-column format allows up to 86 mm (e.g. Fig. 1); two-column format up to 178 mm (e.g. Fig. 2). Please do not provide original graphics files in

Table 6. Two-column table. Seasonal and annual SAT trends (°C decade^{-1}) in the Arctic

Area	1951–2005					1976–2005				
	Dec–Feb	Mar–May	Jun–Aug	Sep–Nov	Annual	Dec–Feb	Mar–May	Jun–Aug	Sep–Nov	Annual
Atlantic region	0.09	0.29	0.10	0.09	0.15	0.470	0.60	0.45	0.53	0.59
Siberian region	0.12	0.29	0.04	0.17	0.16	0.08	0.69	0.29	0.59	0.48
Pacific region	0.45	0.46	0.25	0.26	0.35	0.712	1.08	0.27	0.66	0.52
Canadian region	0.16	0.12	0.14	0.30	0.18	0.20	0.52	0.48	0.94	0.53
Baffin Bay region	−0.02	0.10	0.00	0.15	0.02	0.33	0.62	0.51	0.80	0.57
Arctic 1	0.16	0.21	0.12	0.20	0.18	0.36	200.65	0.42	0.74	0.54
Arctic 2	0.22	0.29	0.14	0.14	0.19	0.38	0.60	0.40	0.51	0.45
Arctic 3	0.28	0.31	0.14	0.13	0.21	0.42	40.53	0.41	0.42	0.43
NH (land + ocean)	0.13	0.13	0.10	0.10	0.12	0.27	0.24	0.25	0.25	0.25

which the figure is a great deal larger or smaller than what you envisage will be the final printed size. To typeset two-column format, add asterisks (`\begin{figure*}...\end{figure*}`) as shown in Fig. 2. We may change the format in-house if necessary. Please note that if you choose to refer to figures using labels, `\caption` must precede `\label`, as in standard LaTeX.

Please send one file for each figure (in other words do not use subfigures) and use a name that clearly identifies it (e.g. '72A712Fig03.eps').

In addition, figures should be eps, ai (illustrator), ps, tif, psd or pdf. Use strong black lines with a width of at least 0.75pt at final printed size (avoid tinting if possible) and SI units in labels. Lettering should ideally be Optima to match the final typeface; Arial or a similar sans serif font for a second choice. Aim to have the final-size lettering at 9pt, if possible. Figures should not be in boxes. The source code for Figs 1 and 2 is shown immediately below the figures.

Equations

We are including some complex equations as examples. Equations should be checked for width by removing the `[review]` option. Note the use of `cases*` in the following equation:

$$\alpha_{t_2} = \begin{cases} \alpha_{t_1} - a_1[\ln(T+1)]\mathrm{e}^{(a_2\sqrt{n})} & n_\mathrm{d} > 0 \quad \text{and} \quad T > 0 \\ \alpha_{t_1} - a_3\mathrm{e}^{(a_2\sqrt{n})} & n_\mathrm{d} > 0 \quad \text{and} \quad T < 0 \\ \alpha_{t_1} + a_4 P_\mathrm{s} & n_\mathrm{d} = 0 \end{cases} \tag{2}$$

Equations should be aligned on the equals signs where possible. Equations that extend beyond the one-column measure should be turned over before an operator.

$$\begin{aligned} l_c = l_0 \left(\frac{\bar{R}_m}{R}\right)^2 \psi^{\frac{P}{P_0 \cos Z}} \\ \times [\cos\beta\, \cos Z + \sin\beta\, \sin Z\, \cos(\psi_\mathrm{sun} - \psi_\mathrm{slope})] \end{aligned} \tag{3}$$

Typesetting upright Greek characters

Normal greek: `$\alpha\beta\gamma\delta$` $\alpha\beta\gamma\delta$

Upright greek: `$\upalpha\upbeta\upgamma\updelta$` $\upalpha\upbeta\upgamma\updelta$

Usual partial: `$\partial$` ∂

Upright partial: `$\uppartial$` $\uppartial$

Marginal notes

The IGS class file redefines the LaTeX command `\marginpar`. If you wish to add a marginal note such as the one alongside this text, you would key `\marginpar{Editor! Help!}`. Marginal notes will be removed before printing.

Editor! Help!

References

All citations in text should include the author name(s) and the year of publication (e.g. 'Smith, 2014'; 'Smith and Jones, 2014'; 'Smith and others, 2015') and have an entry in the reference list.

References should:

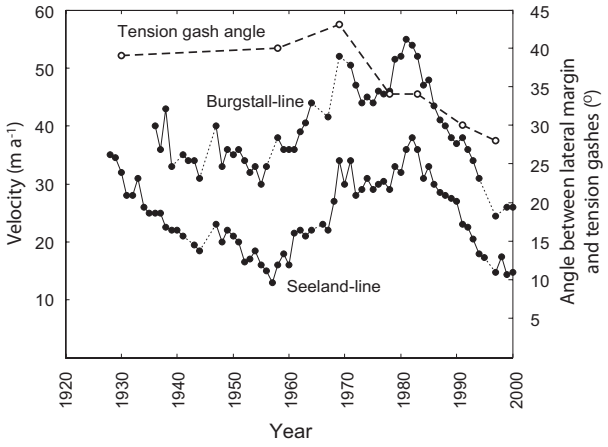

Fig. 1. One-column figures should be ⩽86 mm. Good artwork can make or break a paper. Capitalize the first word of a label and use round not square brackets for units.

be short;

be complete and accurate;

be arranged in alphabetical order by first author's surname;

include too much rather than too little information;

include doi numbers where available (note that older bib databases often included doi's in the page field – in which case they may appear after a comma and without braces);

include works accepted but not published as 'in press';

not include personal communications, unpublished data or manuscript in preparation or submitted for publication, data published on the web (these should be included in the text).

Automatic references using BibTeX

To generate automatic references from a bib database, you must first specify the database (we are using `igsrefs.bib`) and then the IGS bibliography style by placing the following two commands where you would like the references to appear (normally at the end of your paper, before `\end{document}`):

```
\bibliography{igsrefs}
\bibliographystyle{igs}
```

Then run through the following steps:

1. Run your paper through LaTeX.
2. Run BibTeX on your paper.
3. Open the newly-created bbl file containing the cited references and copy the entire contents to just below the `bibliography/bibliographystyle` commands.
4. Then comment them out:

```
%\bibliography{igsrefs}
%\bibliographystyle{igs}
```

5. Run your paper through LaTeX *twice* more.

The IGS do not need your bib or bbl files. Note that BibTeX will lose the second initial in the entry 'Box JE', for example, if it has been typed as '{J.E.} Box' in the bib file. This is because any text in an entry enclosed in { } will be treated as a single unit, and will not be further parsed. Prof. Box's name will typeset correctly if entered as 'J. E. Box' in the bib file.

If you have cited 16 references from the bib database, e.g. (Rignot and Steffen, 2008), (Rignot and others, 2008), (Motyka and others, 2011), (Morlighem and others, 2010), (Morlighem and others, 2011), (Seroussi and others, 2011), (Yan and others, 2013), (Rogozhina and others, 2012), (Hanna and others, 2013), (Goelzer and others, 2013), (Lucas-Picher and others, 2012), (Edwards and others, 2014), (Gladstone and others, 2010), (Morlighem and others, 2013), (Goldberg and Sergienko, 2011) and (Paterson, 1994), the output will be just those 16 references and they will appear at the end of the article.

Citations using natbib commands Note that the standard natbib style file has been modified to fall into line with IGS style. The modified style file is called igsnatbib.sty (included in this distribution), and works exactly the same as natbib.sty. The default IGS house style is (Yan and others, 2013). The following combinations are also available – refer to the natbib documentation if you require any further explanation:

(Yan and others, 2013) `\citep{Yan13}`

(see Yan and others, 2013, p. 34)

```
\citep[see][p.$\,$34]{Yan13}
```

(e.g. Yan and others, 2013) `\citep[e.g.][]{Yan13}`

(Yan and others, 2013, Section 2.3)

```
\citep[Section~2.3]{Yan13}
```

(Yan and others, 2013; Edwards and others, 2014)

```
\citep{Yan13, Edwards14}
```

Yan and others (2013); Edwards and others (2014)

```
\cite{Yan13, Edwards14}
```

Yan and others 2013 `\citealt{Yan13}`

Yan and others (2013) `\cite{Yan13}`

Yan and others, 2013 `\citealp{Yan13}`

Yan and others `\citeauthor{Yan13}`

(2013) `\citeyearpar{Yan13}`

2013 `\citeyear{Yan13}`

ACKNOWLEDGEMENTS

We would like to thank Jason Amundson, Ed Bueler, Andrew Clifton, Gwenn Flowers, Ralf Greve and Doug MacAyeal for their constructive reviews of the IGS class file and guide. Thanks are also due to Patrick Daly who once again helped to generate the latest version of igs.bst.

REFERENCES

(????) *Patran/Nastran, Version 2016/2018*. MSC Software, Santa Ana, California

(????) *Unigraphics NX, Version 12*. Siemens, Munich, Germany

(1994) *British Antarctic Survey: Natural Environment Research Council*. Butterworth-Heinemann, Oxford, 3rd edition

(1998) *Military Handbook Metallic Materials and Elements for Aerospace Vehicle Structures, MIL-HDBK-5H*. Department of Defense

(2018) Part 25 airworthiness standards: Transport category airplanes: Subpart c – structures. *Title 14: Aeronautics and Space, Electronic Code of Federal Regulations: e-CFR*, (8), 8

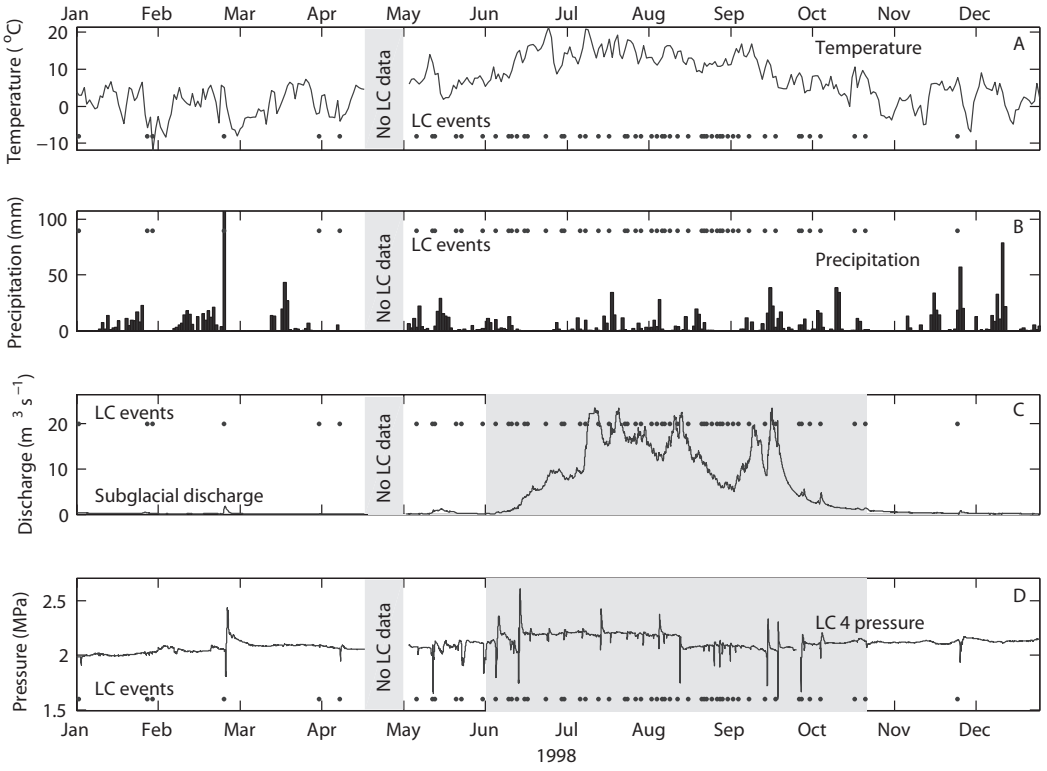

Fig. 2. Two-column figures should be ⩽178 mm. SSA reconstructed components found by projecting the SSA filters found using the whole 2000 traces in Fig. 4, on trace number 1, ordered by magnitude of variance accounted for in the radar trace.

```
\begin{figure*}%fig2, two column
\centering{\includegraphics{72A712Fig02.eps}}
\caption{Two-column figures should be $\leq$178$\,$mm. SSA reconstructed components found by
  projecting the SSA filters found using the whole 2000 traces in Fig.~4, on trace number 1,
  ordered by magnitude of variance accounted for in the radar trace.}
\label{filters}
\end{figure*}
```

Edwards TL, Fettweis X, Gagliardini O, Gillet-Chaulet F, Goelzer H, Gregory JM, Hoffman M, Huybrechts P, Payne AJ, Perego M, Price S, Quiquet A and Ritz C (2014) Effects of uncertainty in surface mass balance-elevation feedback on projections of the future sea level contribution of the Greenland ice sheet. *The Cryosphere*, **8**, 195–208 (doi: 10.5194/tc-8-195-2014)

Gladstone RM, Lee V, Vieli A and Payne AJ (2010) Grounding line migration in an adaptive mesh ice sheet model. *J. Geophys. Res.-Earth*, **115**, F04014 (doi: 0.1029/2009JF001615)

Goelzer H, Huybrechts P, Fürst JJ, Nick FM, Andersen ML, Edwards TL, Fettweis X, Payne AJ and Shannon S (2013) Sensitivity of Greenland ice sheet projections to model formulations. *J. Glaciol.*, **59**(216), 733–749 (doi: 10.3189/2013JoG12J182)

Goldberg DN and Sergienko OV (2011) Data assimilation using a hybrid ice flow model. *The Cryosphere*, **5**, 315–327 (doi: 10.5194/tc-5-315-2011)

Hanna E, Navarro FJ, Pattyn F, Domingues CM, Fettweis X, Ivins ER, Nicholls RJ, Ritz C, Smith B, Tulaczyk S, Whitehouse PL and Zwally HJ (2013) Ice-sheet mass balance and climate change. *Nature*, **498**, 51–59 (doi: 10.1038/nature12238)

Lucas-Picher P, Wulff-Nielsen M, Christensen JH, Adalgeirsdóttir G, Mottram RH and Simonsen SB (2012) Very high resolution regional climate model simulations over Greenland: identifying added value. *J. Geophys. Res.*, **117**, D02108 (doi: 10.1029/2011JD016267)

Morlighem M, Rignot E, Seroussi H, Larour E, Dhia HB and Aubry D (2010) Spatial patterns of basal drag inferred using control methods from a full-Stokes and simpler models for Pine Island Glacier, West Antarctica. *Geophys. Res. Lett.*, **37**, L14502 (doi: 10.1029/2010GL043853)

Morlighem M, Rignot E, Seroussi H, Larour E, Dhia HB and Aubry D (2011) A mass conservation approach for mapping glacier ice thickness. *Geophys. Res. Lett.*, **38**, L19503 (doi: 10.1029/2011GL048659)

Morlighem M, Seroussi H, Larour E and Rignot E (2013) Inversion of basal friction in Antartica using exact and incomplete adjoints of a higher-order model. *J. Geophys. Res.*, **118**, 1746–1753 (doi: 10.1002/jgrf.20125)

Motyka RJ, Truffer M, Fahnestock M, Mortensen J, Rysgaard S and Howat I (2011) Submarine melting of the 1985 Jakobshavn Isbrae floating tongue and the triggering of the current retreat. *J. Geophys. Res.*, **116**, F01007 (doi: 10.1029/2009JF001632)

Paterson WSB (1994) *The physics of glaciers*. Butterworth-Heinemann, Oxford, 3rd edition

Rignot E and Steffen K (2008) Channelized bottom melting and stability of floating ice shelves. *Geophys. Res. Lett.*, **35**, L02503 (doi: 10.1029/2007GL031765)

Rignot E, Box JE, Burgess E and Hanna E (2008) Mass balance of the Greenland ice sheet from 1958 to 2007. *Geophys. Res. Lett.*, **35**, L02502 (doi: 10.1029/2008GL035417)

Rogozhina I, Hagedoorn JM, Martinec Z, Fleming K, Soucek O, Greve R and Thomas M (2012) Effects of uncertainties in the geothermal heat flux distribution on the Greenland ice sheet: an assessment of existing heat flow models. *J. Geophys. Res.*, **117**, F02025 (doi: 10.1029/2011JF002098)

Seroussi H, Morlighem M, Rignot E, Larour E, Aubry D, Dhia HB and Kristensen SS (2011) Ice flux divergence anomalies on 79north glacier, Greenland. *Geophys. Res. Lett.*, **38**, L09501 (doi: 10.1029/2011GL047338)

Yan Q, Zhang Z, Gao Y, Wang H and Johannessan OM (2013) Sensitivity of the modeled present-day Greenland ice sheet to climatic forcing and spin-up methods and its influence on future sea level projections. *J. Geophys. Res. Earth Surf.*, **118**, 2174–2189 (doi: 10.1002/jgrf.20156)

APPENDIX

Start an appendix by typing `\appendix\section{Appendix}`. Appendices appear after the references. Equation numbers automatically start again with (4).

$$2\eta\kappa\frac{\partial\bar{u}}{\partial t} + \rho_{\mathrm{r}} g\bar{u} + D\kappa^4\bar{u} = \bar{\sigma}_{zz}. \tag{4}$$

HANDLING MORE THAN ONE APPENDIX

Use the following code to achieve heading APPENDIX A followed by APPENDIX B and APPENDIX C, with appropriate equation numbers:

```
\appendix
\section{Appendix A}

\setcounter{equation}{0}
\renewcommand\theequation{B\arabic{equation}}
\section{Appendix B}

\setcounter{equation}{0}
```

```
\renewcommand\theequation{C\arabic{equation}}
\section{Appendix C}
```